HHS Public Access

Author manuscript

Nucl Med Biol. Author manuscript; available in PMC 2017 January 20.

Published in final edited form as:

Nucl Med Biol. 2016 December ; 43(12): 743–751. doi:10.1016/j.nucmedbio.2016.08.018.

Evaluation of pancreatic VMAT2 binding with active and inactive enantiomers of ^{18}F-FP-DTBZ in baboons

Mika Naganawa[#a,*], **Shu-fei Lin**[#a], **Keunpoong Lim**[a], **David Labaree**[a], **Jim Ropchan**[a], **Paul Harris**[b], **Yiyun Huang**[a], **Masanori Ichise**[b], **Richard E. Carson**[a], and **Gary W. Cline**[a]

[a]Yale University, 801 Howard Avenue, PO Box 208048, New Haven, CT, United States, 06520

[b]Columbia University, New York, NY, United States

[#] These authors contributed equally to this work.

Abstract

Introduction—^{18}F-Fluoropropyl-(+)-dihydrotetrabenazine (^{18}F-FP-(+)-DTBZ) is a vesicular monoamine transporter type 2 (VMAT2) radiotracer for positron emission tomography (PET) imaging to quantify human β-cell mass. Renal cortex and spleen have been suggested as reference regions, however, little is known about ^{18}F-FP-(+)-DTBZ binding in these regions including the fraction of radiometabolite. We compared the kinetics of ^{18}F-FP-(+)-DTBZ and its inactive enantiomer ^{18}F-FP-(−)-DTBZ in baboons, estimated the non-displaceable binding (V_{ND}) of the tracers, and used *ex vivo* studies to measure radiometabolite fractions.

Methods—PET scans were conducted for up to 4 h with (+) and (−) enantiomers. Displacement experiments using unlabeled (+) and (−) enantiomers of FP-DTBZ and fluvoxamine (to evaluate sigma-1 receptor binding) were performed. SUV curves were used to calculate displacement values in the pancreas, renal cortex, and spleen. Distribution volumes (V_T) were computed, and three approaches for calculation of V_{ND} were compared: (1) ^{18}F-FP-(+)-DTBZ reference V_T, (2) ^{18}F-FP-(−)-DTBZ pancreatic V_T, and (3) a scaled ^{18}F-FP-(+)-DTBZ reference V_T values. *Ex vivo* study was conducted to measure radiometabolite fraction in homogenized tissue samples from baboons at 90 min post-injection.

Results—Spleen uptake was lowest for both tracers. Highest uptake was in the pancreas with ^{18}F-FP-(+)-DTBZ and renal cortex with ^{18}F-FP-(−)-DTBZ. Substantial displacement effect was observed only with unlabeled FP-(+)-DTBZ in the ^{18}F-FP-(+)-DTBZ studies. Radiometabolite fraction was higher in the renal cortex than the spleen. Approaches (1) and (3) with spleen to estimate V_{ND} provided lowest inter-subject variability of BP_{ND}.

Conclusions—V_T differences among organs and between enantiomers indicated that scaling of reference region values is needed for quantification of VMAT2 binding in the pancreas with ^{18}F-FP-(+)-DTBZ. Since the kidney PET signal has greater partial volume averaging and more radiometabolites, the spleen was considered a more practical candidate for use as a scaled-reference region in the quantification of ^{18}F-FP-(+)-DTBZ in the pancreas.

[*]Corresponding author. Tel.: +1 203 737 5582; fax: +1 203 785 3107. mika.naganawa@yale.edu (M. Naganawa). .

Supplementary data to this article can be found online at http://dx.doi.org/10.1016/j.nucmedbio.2016.08.018.

Keywords

Vesicular monoamine transporter type 2; β-cell mass; PET; ^{18}F-FP-(+)-DTBZ; ^{18}F-FP-(−)-DTBZ; Pancreas non-displaceable binding

1. Introduction

Our current understanding of the natural history of β-cell mass (BCM) in relation to the onset and progression of either type-1 (T1DM) or type-2 diabetes mellitus (T2DM) is based largely on indirect *in vivo* measures of endocrine/metabolic surrogates of BCM and/or limited autopsy studies [1,2]. In addition, monitoring β-cell survival during drug and cell-based therapies remains a challenge because of lack of a technique to monitor and quantify BCM *in vivo*. Measurement of insulin secretory capacity is currently used as a surrogate marker of BCM, which may not accurately reflect total BCM. Serum insulin and C-peptide concentrations can provide only an imprecise reflection of BCM as changes in the ability of glucose to stimulate insulin secretion in the progression to diabetes may be due to loss of function and/or mass [3]. In order to assess BCM, a biomarker that is independent of function is required. Vesicular monoamine transporter type 2 (VMAT2) is predominately expressed within insulin-positive human pancreatic β-cells [4–6]. VMAT2 expression was strongly correlated with β-cell density [7], with a minor contribution from VMAT2 expression in pancreatic polypeptide (PP) cells. Results from recent studies have provided support for the use of positron emission tomography (PET) with the radioligand ^{18}F-fluoropropyl-(+)-dihydrotetrabenazine (^{18}F-FP-(+)-DTBZ), a biomarker targeting the VMAT2, to noninvasively estimate human BCM [8].

^{18}F-FP-(+)-DTBZ PET images have shown excellent pancreatic uptake in humans [8], baboons [9], and rodents [10]. However, the intense PET signal consists of not only specific VMAT2 binding in the β-cells, but also specific binding to the PP cells and non-specific binding to pancreatic tissue. To accurately estimate VMAT2 specific binding, we must have knowledge of the non-displaceable (=non-specific + free) binding component of ^{18}F-FP-(+)-DTBZ in the pancreas, and/or in a suitable reference tissue where specific VMAT2 binding is absent. The radiotracer binding to PP cells is not distinguishable from the binding to β-cells, however its contribution to total pancreas radiotracer binding is expected to be minimal due to the localized distribution and overall low-density of PP cells within the pancreas. However, since the β-cells are dispersed throughout the pancreas, no reference tissue free of VMAT2 can be defined within the pancreas. The non-displaceable binding component of ^{18}F-FP-(+)-DTBZ in the rodent pancreas has been estimated at about 30% of the total by pre-treatment [10] or displacement [11] with the unlabeled VMAT2 antagonist tetrabenazine or FP-(+)-DTBZ. Importantly, the renal cortex was shown to be a potential reference tissue, as the total uptake in this region was found to be similar to the non-displaceable binding in the pancreas. In a previous human study [8], the spleen was also suggested as a possible reference tissue. The spleen could potentially be superior to the kidneys as a general reference region for estimating BCM in the pancreas in healthy subjects and patients with T1DM, since renal uptake is affected by diabetes. In this study [8], long-standing T1DM patients showed a smaller reduction in specific VMAT2 binding potentials

(BP_{ND}) than expected, whereas functional BCM was almost depleted. The apparent overestimation of BP_{ND} may be caused, at least in part, by the reference region, if the non-displaceable distribution volume (V_{ND}) was underestimated.

Thus, further studies are needed to validate the selection of a reference region in humans. Here, we exploit differences in VMAT2-binding of the stereoisomers of ^{18}F-FP-DTBZ to identify a suitable reference region for quantification of non-displaceable pancreatic binding. The binding of ^{18}F-FP-(+)-DTBZ to VMAT2 is stereospecific, such that the (−)-enantiomer has very low affinity for VMAT2 (K_i > 3000 nM) compared to the (+)-enantiomer (K_i = 0.10 nM) [12], and can potentially be used to directly estimate non-displaceable binding within the pancreas and reference regions. In order to assess the validity of the use of ^{18}F-FP-(−)-DTBZ to measure non-displaceable binding in human pancreas, we first carried out a proof of concept study in non-human primates to evaluate the specific and non-displaceable binding components for both the (+)- and (−)- enantiomers of ^{18}F-FP-DTBZ.

Harris et al. [9] have previously conducted baboon PET imaging using both the (+)- and (−)-enantiomers of ^{18}F-FP-DTBZ, and found that the distribution volume (V_T) values for the renal cortex and spleen measured with ^{18}F-FP-(+)-DTBZ were similar to the V_T values in the pancreas by ^{18}F-FP-(−)-DTBZ. Therefore, they concluded that the V_{ND} of the pancreas can be estimated by the V_T of the renal cortex or spleen with ^{18}F-FP-(+)-DTBZ. Based on those results, any overestimation of ^{18}F-FP-(+)-DTBZ BP_{ND} in the human pancreas was not due to the underestimation of V_{ND} by using the renal cortex as reference region.

In addition to a VMAT2 binding site of ^{18}F-FP-(+)-DTBZ, a low affinity but high capacity ^{18}F-FP-(+)-DTBZ binding at sigma receptors in rat pancreatic exocrine and islet cell homogenates has been reported [13]. Given that both FP-(+)-DTBZ and FP-(−)-DTBZ display a weak affinity for binding to the sigma-1 receptors *in vitro* (K_i of 95 and 110 nM, respectively) [13], the total PET signal detected in target tissues, *e.g.* pancreas, kidney, and spleen, may be partially attributed to a specific sigma receptor binding.

In this present study, we conducted displacement studies of ^{18}F-FP-(+)-DTBZ and ^{18}F-FP-(−)-DTBZ with both unlabeled enantiomers of FP-DTBZ, and with fluvoxamine, a sigma-1 receptor agonist in baboons. Three methods are reported to define V_{ND} to calculate BP_{ND}. Further, *ex vivo* studies with both (+)- and (−)- enantiomers of ^{18}F-FP-DTBZ in three baboons were carried out to examine whether the regional uptake reflects only the authentic parent radiotracer in target tissues.

2. Materials and methods

2.1. Synthesis of ^{18}F-FP-(+)-DTBZ and ^{18}F-FP-(−)-DTBZ

^{18}F-FP-(+)-DTBZ is synthesized by ^{18}F-fluorination of the mesylate precursor, 9-(3-methanesulfonyloxypropoxy)-1,3,4,6,7,11b-hexahydro-10-methoxy-3-(2-methylpropyl) (2R, 3R,11bR)-2H-benzo[a]quinolizin-2-ol. Aqueous ^{18}F-fluoride was produced with a 30 min beam at 35 μA from a GE PETtrace cyclotron (GE; Milwaukee, WI) *via* the ^{18}O(p,n)^{18}F reaction. Preparation of ^{18}F-FP-(+)-DTBZ was carried out in a TRACERLab™ FX_{F-N} automated synthesis module (GE Medical Systems).

Aqueous ^{18}F-fluoride produced from the cyclotron was loaded onto a Chromafix 30-PS-HCO_3 separation cartridge and eluted into the graphite reaction vessel with a solution of 7.14 mg Kryptofix K_{222} and 0.74 mg K_2CO_3 in 1 mL of CH_3CN/water (1:0.4, *v/v*). The solvent was evaporated at 70 °C at reduced pressure (~33 kPa) under an argon stream for 5 min. A 1 mL aliquot of CH_3CN was added and azeotropic evaporation resumed at 70 °C for 3 min, then a second 1 mL aliquot of CH_3CN was added and evaporation continued at 100 °C for another 5 min. The argon flow was stopped and any remaining solvent was evaporated at 100 °C at reduced pressure (~8 kPa) for an additional 5 min leaving a dried residue. After cooling to 60 °C, the radiolabeling precursor (0.5 ± 0.1 mg) in 0.5 mL mixture of DMF/acetonitrile (3/2, *v/v*) was added. The reaction vessel is sealed, stirred and heated at 110 °C for 7 min, then cooled to 50 °C. The reaction mixture was diluted with H_2O (6.75 mL) and loaded onto a C-18 SepPak Light cartridge. The reaction vessel was rinsed with another portion of H_2O (6.75 mL) and the rinse was also passed through the SepPak Light cartridge. The SepPak cartridge was eluted with 1 mL of EtOH into a receiving vial containing 3 mL of semipreparative HPLC mobile phase. The content in the receiving vial was loaded onto a semi-preparative column (Phenomenex Luna C18(2), 10 μm, 10 × 250 mm), which was eluted at a flow rate of 2.5 mL/min with a mixture of 40% acetonitrile and 60% 0.1 M aqueous ammonium formate (*v/v*) containing sodium ascorbate (5 g/L mobile phase). The eluent was monitored by a UV detector and a radioactivity detector. The product fraction was collected, diluted with H_2O (15 mL) and passed through a second C18 SepPak Light cartridge. The SepPak cartridge was rinsed with 0.5% sodium ascorbate solution (15 mL). ^{18}F-FP-(+)-DTBZ was eluted off the SepPak with 1 mL of absolute ethanol (USP), followed by 3 mL of 0.5% sodium ascorbate in USP saline, into a product vial containing 7 mL of 0.5% sodium ascorbate in USP saline. This mixture was then passed through a sterile membrane filter (0.22 μm) for terminal sterilization and collected in a sterile vial to afford a formulated solution ready for dispensing and injection. Total synthesis time was about 80 min from end of beam (EOB).

A portion of the final formulated product solution (~1 mL) was used for quality control tests. For determination of chemical purity, radio-chemical purity, and specific radioactivity, an amount (5–100 μL) of the solution was withdrawn into an HPLC syringe and the amount of radioactivity (MBq) assayed using a dose calibrator (Capintec). The solution was then analyzed by HPLC (column: Phenomenex Luna C18(2), 5 μm, 100 Å, 4.6 × 250 mm; mobile phase: 31% acetonitrile and 69% 0.1 M aqueous ammonium formate solution; flow rate: 2 mL/min; UV detector wavelength: 280 nm). The area of the UV peak associated with FP-(+)-DTBZ was compared to a pre-defined standard mass curve to determine the mass (nmol). The specific activity (MBq/nmol) of ^{18}F-FP-(+)-DTBZ was calculated as the ratio between the amount of radioactivity (MBq) and the amount of mass (nmol). Additional quality control tests were performed before the product batch was released for use.

Synthesis procedures of ^{18}F-FP-(−)-DTBZ were the same as those for ^{18}F-FP-(+)-DTBZ, except using the (−)-enantiomer of the radiolabeling precursor.

Radiochemical purity of the ^{18}F-FP-(+)-DTBZ and ^{18}F-FP-(−)-DTBZ final product solution was >97%. Specific activities of ^{18}F-FP-(+)-DTBZ and ^{18}F-FP-(−)-DTBZ at the end of synthesis were 280 ± 96 MBq/nmol (n = 8) and 351 ± 88 MBq/nmol (n = 3), respectively.

2.2. PET studies in baboons

Eleven PET imaging experiments were performed in four female adult baboons (baboons A, B, C, D, age, 7.8 ± 1.8 years old; weight, 16.1 ± 4.1 kg) according to a protocol approved by the Yale University Institutional Animal Care and Use Committee. Animals were initially sedated with ketamine (10 mg/kg) and glycopyrrolate (0.01 mg/kg) and subsequently anesthetized with isoflurane (1.5–2.5%). Vital signs (heart rate, blood pressure, respirations, and electrocardiogram) were continuously monitored during the procedure.

PET scans were acquired on the EXACT HR+ scanner (Siemens Medical Solutions, Knoxville, TN, USA). The baboons underwent PET scans for 3–4 h after injection of either ^{18}F-FP-(+)-DTBZ or ^{18}F-FP-(−)-DTBZ. The tracers were administered as a 3-min bolus. For both tracers, control and displacement scans were performed on separate days. For ^{18}F-FP-(+)-DTBZ, displacement scans were performed with unlabeled FP-(+)-DTBZ (0.25 or 0.5 mg/kg), FP-(−)-DTBZ (0.5 mg/kg), or fluvoxamine (3 mg/kg) administered intravenously over 5 min at 90 min post-injection. For ^{18}F-FP-(−)-DTBZ, displacement scans were performed with unlabeled FP-(+)-DTBZ (0.5 mg/kg) and unlabeled FP-(−)-DTBZ (0.5 mg/kg). See Table 1 for a summary of experiment parameters. Control scans were obtained under identical protocols as those used for the displacement scans, with the exception that saline was injected at 90 min after radioligand injection.

PET images were reconstructed with attenuation and scatter correction using an ordered subset expectation maximization algorithm with 4 iterations and 16 subsets. Rigid body motion toward the ventral side along the dorsoventral axis occurred after the displacement scans with fluvoxamine in both baboons. A six-parameter mutual information algorithm [14] was applied to the scans to eliminate this rigid motion.

Three regions of interest (ROIs) were manually drawn on the summed PET images from 0 to 90 min post tracer injection to generate time–activity curves (TACs) for renal cortex, spleen, and pancreas.

2.3. Input function measurement

Arterial samples (0.5 to 3.0 mL per sample, total amount: 22.5 mL) were collected manually at selected time points (0.75, 1.5, 2.25, 3, 3.75, 4.5, 5.25, 6, 8, 10, 15, 20, 30, 45, 60, 75, 90, 105, 120, 150, and 180 min after radiotracer injection). For scans with displacement at 90 min, frequent blood sampling between 90 and 100 min was conducted to detect any change in plasma radioactivity due to the displacement. The eight samples drawn at 3, 8, 15, 30, 60, 90, 120, and 180 min were analyzed for radioactive metabolites using an automatic column-switching high-performance liquid chromatography (HPLC) system with a Phenomenex Luna C18(2) analytical column (5 μm, 4.6 × 250 mm) as described in our previous publication [8] eluting a mobile phase of 40% acetonitrile and 60% 0.1 M ammonium formate (*v/v*) at a flow rate of 1.50 mL/min. The unmetabolized parent fraction was determined as the ratio of the radioactivity corresponding to the parent (retention time of 9–11 min) to the total amount of radioactivity collected, fitted with an inverted gamma function.

2.4. Quantitative analysis

Outcome measures were derived with kinetic analysis of the regional TACs using the arterial plasma TAC as input function. One- and two-tissue compartment models (1TC, 2TC), and the multilinear analysis-1 (MA1) method [15] were applied to TACs (from control scans) to calculate the distribution volume (V_T) [16] for different scan durations. V_T of ^{18}F-FP-(+)-DTBZ and ^{18}F-FP-(−)-DTBZ is indicated as $V_T(+)$ and $V_T(-)$, respectively. Similarly, V_{ND} of ^{18}F-FP-(+)-DTBZ and ^{18}F-FP-(−)-DTBZ is indicated as $V_{ND}(+)$ and $V_{ND}(-)$, respectively.

For displacement scans, the %displacement in SUV was calculated by comparing the average SUV after displacement with the predicted value in the absence of displacement, as follows:

$$\%\text{Dispplacement}=100\times\left(1-\frac{D_{post}}{D_{pre}\times\frac{C_{post}}{C_{pre}}}\right)$$

where C and D denote the averaged SUV in the control and displacement scans, respectively. The subscripts ‘pre’ and ‘post’ represent times pre- and post-displacement, specifically 60–90 min and 120–150 min, respectively.

Although both renal cortex and spleen have been proposed as a reference region, there has been no definitive evidence to support the usage of these reference regions. We compared three methods to determine V_{ND} to calculate BP_{ND}. In all three methods, specific binding is assumed to be negligible in all regions for ^{18}F-FP-(−)-DTBZ (see Results), and to be negligible in non-pancreatic regions for ^{18}F-FP-(+)-DTBZ (see Results). The first method is to use the spleen as a conventional reference region, measured with ^{18}F-FP-(+)-DTBZ (*i.e.*, $V_T(+)$ in spleen is assumed to be equal to $V_{ND}(+)$ in pancreas). In the second method, pancreatic $V_T(-)$ is assumed to be equal to $V_{ND}(+)$ in pancreas. With this method, a pair of scans (one with each enantiomer) is always needed. In the third method, V_{ND} is not assumed to be uniform across regions for either enantiomer, but the relative regional profile of V_{ND} is assumed to be similar for both enantiomers: i.e., the ratio $V_{ND}(-,\text{spleen})/V_{ND}(-,\text{pancreas})$ is assumed to be equal to the ratio $V_{ND}(+,\text{spleen})/V_{ND}(+,\text{pancreas})$. Thus, after measuring the ratio, $V_T(-,\text{spleen})/V_T(-,\text{pancreas})$ (denoted α_{spleen}), $V_{ND}(+,\text{pancreas})$ can be estimated as $V_T(+,\text{spleen})/\alpha_{spleen}$. With this method, ^{18}F-FP-(−)-DTBZ scans are not needed if the scaling factor, α_{spleen}, is reproducible across scans and animals.

Methods one and three were also tested using the renal cortex instead of the spleen as a reference tissue. These methods were applied to 90 min of data (including displacement studies). All modeling was performed with in-house programs written with IDL 8.0 (ITT Visual Information Solutions, Boulder, CO, USA).

2.5. Tissue radiometabolite measurement

Three baboons were euthanized 90 min after injection of 11.6 ± 0.1 MBq/kg of ^{18}F-FP-(+)-DTBZ (baboons C and E) or 10.0 MBq/kg ^{18}F-FP-(−)-DTBZ (baboon F). Organ samples

were taken from pancreas (head, uncinate, neck, body, and tail), bilateral renal cortices, spleen, and liver. The brain was also harvested and dissected for the studies with ^{18}F-FP-(+)-DTBZ. The blood and organ samples were weighed and counted. Blood samples were analyzed using the automatic column-switching HPLC method as described above. Organ samples were first denatured with cold methanol (4 °C) in volumes equivalent to the tissue samples and homogenized with the Kinematica Polytron PT1200 E homogenizer (Luzern, Switzerland). Additional amounts (up to a half of the homogenate volume) of saline–methanol mixture (1:1, *v/v*) were added to homogenate samples deemed too thick for homogenization. The homogenates were centrifuged at 4 °C for 10 min at 14,000 rpm with an Eppendorf 5417R benchtop centrifuge (Hauppauge, NY, USA) to precipitate the proteins. Activities in the supernatant and protein pellets were measured and up to 1.0 mL of the supernatant was analyzed by reverse phase analytical HPLC (column: Phenomenex Luna C18(2) analytical column (5 μm, 4.6 × 250 mm); mobile phase: 60% 0.1 M ammonium formate and 40% acetonitrile (*v/v*); flow rate: 1.5 mL/min) to determine the fractions of parent tracer and metabolites.

3. Results

3.1. Plasma analysis

For both radiotracers, the unmetabolized fraction curves were similar between the control and displacement scans. Fig. 1 shows mean unmetabolized fraction curves for ^{18}F-FP-(+)-DTBZ and ^{18}F-FP-(−)-DTBZ across all scans. Parent fractions for ^{18}F-FP-(+)-DTBZ were 55 ± 9%, 18 ± 4%, 11 ± 1%, 9 ± 2%, and 6% at 8 min, 30 min, 60 min, 90 min, and 240 min post-injection, respectively. Parent fractions for ^{18}F-FP-(−)-DTBZ were 49 ± 6%, 14 ± 1%, 10 ± 1%, 10 ± 1%, and 7% at 8 min, 30 min, 60 min, 90 min, and 240 min post-injection, respectively. Plasma TACs for both radiotracers showed a similar pattern.

3.2. Uptake of two enantiomers of ^{18}F-FP-DTBZ

The doses of ^{18}F-FP-(+)-DTBZ and ^{18}F-FP-(−)-DTBZ were 11.9 ± 0.8 and 11.2 ± 2.5 MBq/kg, respectively, and injected mass doses were 0.016 ± 0.004 and 0.021 ± 0.005 μg/kg, respectively. Figs. 2A, B and 3 show SUV images and regional TACs in control scans with ^{18}F-FP-(+)-DTBZ and ^{18}F-FP-(−)-DTBZ. Uptake of ^{18}F-FP-(−)-DTBZ in all regions peaked at ~5 min post-injection and then rapidly decreased. Similar uptake patterns were seen with ^{18}F-FP-(+)-DTBZ in the renal cortex and spleen. On the other hand, pancreatic uptake of ^{18}F-FP-(+)-DTBZ peaked at around 50 min post-injection and cleared very slowly.

3.3. Kinetic model assessment

The quality of curve fitting for both radiotracers was better with the 2TC and MA1 models than the 1TC model, based on clear lack of fit for 1TC (Fig. 3). Note that the blood volume was not included in the models. The 1TC and 2TC models with correction for blood volume were also applied to the TACs. Lack of fits were still seen in the spleen and renal cortex using the 1TC model and the fitted blood volume value was implausible (> 100%). Blood volume varied over different scans (0–26% for ^{18}F-FP-(+)-DTBZ and 25–51% for ^{18}F-FP-(−)-DTBZ) in the pancreas. Using the 2TC model, the blood volume was 0% in most scans in the pancreas for both enantiomers and varied between two enantiomers in the spleen (33–

86% for ^{18}F-FP-(+)-DTBZ and 0–60% for ^{18}F-FP(−)-DTBZ) and renal cortex (54–92% for ^{18}F-FP-(+)-DTBZ and 0–73% for ^{18}F-FP-(−)-DTBZ). Therefore, the blood volume in each organ cannot be estimated based on kinetic analyses of these tracers. For ^{18}F-FP-(+)-DTBZ, the 2TC and MA1 models produced high V_T values in the pancreas that increased with longer scan duration. For both radio-tracers, the parent fraction in the plasma decreased quickly to ~10% until 60 min post-injection and decreased slowly to 6–7% at 240 min post-injection. This means that the parent radiotracer is still available in the plasma even at the end of scan. Given the parent fraction data and no/negligible metabolites in the pancreas tissue at 90 min post-injection (shown below), the increase in the pancreas V_T(+) is attributed to the slow kinetics of the radiotracer in the pancreas; thus an accurate V_T cannot be determined with a shorter scan. Summarized in Table 2 are V_T values derived with the MA1 model (t^* = 40 min) using 1.5 h of data from the control and displacement scans, as well as 2 h, 3 h, and 4 h of data from the control scans. For ^{18}F-FP-(−)-DTBZ, MA1 V_T values were highest in the renal cortex, followed by the pancreas, and lowest in the spleen. In the spleen and pancreas, V_T estimates were stable and did not change with longer scan duration, while in the renal cortex V_T estimates increased slightly. In the renal cortex and spleen, ^{18}F-FP-(+)-DTBZ V_T values were higher than those of ^{18}F-FP-(−)-DTBZ.

3.4. Displacement by two enantiomers of FP-DTBZ and fluvoxamine

Figs. 2C, D, and 4 show SUV images and pancreatic TACs from the displacement experiments. Quantified displacement data in the pancreas, spleen and renal cortex are summarized in Table 3. The displacement with unlabeled FP-(+)-DTBZ resulted in a substantial decrease in ^{18}F-FP-(+)-DTBZ pancreatic binding (24% for the 0.25 mg/kg dose and 48% for the 0.5 mg/kg dose, Fig. 4A), but did not reduce ^{18}F-FP-(+)-DTBZ binding in the renal cortex or spleen (−9 to 9%). In contrast, the SUV of ^{18}F-FP-(+)-DTBZ did not decrease substantially by displacement with unlabeled FP-(−)-DTBZ (1 to 7%, Fig. 4B). The SUV of ^{18}F-FP-(−)-DTBZ changed by less than 15% after displacement with unlabeled FP-(+)-DTBZ (−11 to +14%, Fig. 4E) or unlabeled FP-(−)-DTBZ (−1 to +12%, Fig. 4F). A rigid body motion occurred after fluvoxamine displacement in both baboons (Supplemental Fig. 1 in the online version at http://dx.doi.org/10.1016/j.nucmedbio.2016.08.018A and B). After motion correction, in which all frames were co-registered and resliced to match the summed image from 0 to 90 min post-injection, a small motion was still visible in the dynamic images and in the pancreatic TACs as a slight bump (Fig. 4C and D). Nonetheless, fluvoxamine had a negligible effect on ^{18}F-FP-(+)-DTBZ binding (−11 to +9% change in SUV, Fig. 4C and D), suggesting little or no specific binding of ^{18}F-FP-(+)-DTBZ to sigma-1 receptors.

3.5. Non-displaceable binding estimation

Estimated V_{ND} and BP_{ND} values using the three methods with 2 different reference regions are summarized in Table 4. In all methods, pancreatic BP_{ND} was calculated as V_T(+, pancreas)/V_{ND} − 1. In method 1, V_T(+, spleen) or V_T(+, renal cortex) was used as V_{ND}. In method 2, V_T(−, pancreas) was used as V_{ND}. In method 3, V_T(+, spleen)/α_{spleen} or V_T(+, renal cortex)/α_{renal} was used as V_{ND}. ^{18}F-FP-(−)-DTBZ V_T in the renal cortex was higher than that in the spleen. As a result, in method 1, pancreatic BP_{ND} using spleen as a reference region (BP_{ND}(ref: spleen, method 1)) was twice as large as BP_{ND}(ref: renal cortex, method

1). Although the coefficient of variation (COV) of V_{ND} showed a similar level between spleen (29%) and renal cortex (27%), the COV of BP_{ND}(ref: spleen, method 1) was much smaller than that of BP_{ND}(ref: renal cortex, method 1). Using method 2, pancreas V_T measured with ^{18}F-FP-(−)-DTBZ was used as V_{ND}. Since V_T(−) in pancreas was lower than V_T(+) in spleen or renal cortex, BP_{ND} estimated with method 2 was higher than BP_{ND} estimated with method 1. Additionally, the COV of pancreatic BP_{ND}(+) showed the highest variability among all methods. For method 3, the scale factor α had a very small COV with that of α_{spleen} smaller than that of α_{renal}. Using αspleen in method 3, COV values of BP_{ND} were similar to those from method 1.

3.6. Tissue radiometabolite measurement

Listed in Table 5 are the SUVs and parent fractions measured with tissue and plasma samples taken at 90 min post-injection. The corresponding HPLC chromatograms are shown in Fig. 5. Among sampled organs, the highest SUV of ^{18}F-FP-(+)-DTBZ was detected in the pancreas (head, uncinate, neck, body, and tail), caudate and putamen, followed by the renal cortices, lower uptake in the liver and spleen, and the lowest in the frontal cortex and cerebellum. A very small fraction of radiometabolites was detected in the pancreas as a whole (>97% of parent fraction). There were no differences in parent fraction between left and right renal cortices. The contribution of radiolabeled metabolites of ^{18}F-FP-(+)-DTBZ to the total radiotracer counts was negligible in the pancreas (~1%), small in the spleen (~6%), but substantial in the kidney (~30%). In contrast, the parent accounted for only ~10% of the total activity in the plasma at the same time point. For ^{18}F-FP-(−)-DTBZ, the SUV in the renal cortices was the highest, followed by the liver, and the lowest in the spleen and pancreas as a whole. Parent fractions in all regions were lower (25–63%) in comparison to ^{18}F-FP-(+)-DTBZ. Radiolabeled metabolites of ^{18}F-FP-(−)-DTBZ made significant contributions to the PET signal in all regions, including the pancreas (~44%), spleen (~47%), and kidney (~72%).

4. Discussion

We conducted PET imaging studies of two radiolabeled enantiomers, ^{18}F-FP-(+)-DTBZ and ^{18}F-FP-(−)-DTBZ in baboons, in an effort to profile and quantify the non-displaceable binding component of ^{18}F-FP-(+)-DTBZ, which has been used to image VMAT2 in the pancreas as a surrogate biomarker for BCM. Displacement experiments with each radiolabeled enantiomer were conducted with unlabeled FP-(+)-DTBZ and FP-(−)-DTBZ, and with fluvoxamine for ^{18}F-FP-(+)-DTBZ. We evaluated three methods to estimate non-displaceable binding and compared the magnitude and inter-subject variability of BP_{ND}. Also, to determine if any radiolabeled metabolites contributed to the PET signal in target organs, we performed an *ex vivo* study to measure the fractions of parent radioligand and their radioactive metabolites in the pancreas, spleen, and kidney.

The radiotracer ^{18}F-FP-(+)-DTBZ binds to VMAT2 in beta-cell (target) as well as that in PP cells (off-target). The binding to PP cells leads to the overestimation of BCM measurement. Approximately 40% of PP cells express VMAT2 while 90% of β-cells express VMAT2 [7]. A postmortem pancreas study in healthy human subjects [17] found that 90% of the

pancreas was characterized as poor in the PP cells (volume density of 0.03%) and 10% was rich in the PP cells (volume density of 2.3%). The volume density of β-cells was 1.2 to 1.8% in the PP-poor region and 0.5% in the PP-rich region. VMAT2-positive PP cell density can be estimated to represent 0.10% of the volume of the pancreas, compared to VMAT2-positive β-cell density of 1.0 to 1.5%. Therefore, the tracer binding to PP cells can be estimated to be minor (7–10%) relative to that of β-cells. Also, a recent study showed that the PP-rich region was more narrowly restricted to the ulcinate process within the head region [18], which suggests that tracer binding to PP cells in the majority of the pancreas would be even lower.

As expected, substantial displacement was observed in the pancreatic SUV curves only in the scans with ^{18}F-FP-(+)-DTBZ following a displacement dose of unlabeled FP-(+)-DTBZ (Fig. 4). Nearly identical TACs were observed for the control and displacement ^{18}F-FP-(−)-DTBZ scans (Fig. 4E and F) suggesting minimal, or no displacement. However, the calculated displacement values (Table 3) differ from each other: 14% for Fig. 4E and −1% for Fig. 4F, and, in the former case, could be suggestive of slight displacement. This apparent discrepancy between conclusions based on the visual inspection of SUV curves vs. displacement values derived from quantitative analysis results from the design of our scan protocol. The use of the displacement index computed in this study assumes a perfect test and retest reproducibility in the curve shape between studies, and as a result, a perfect reproducibility in the shape of the input functions is also required between the scans. Indeed, in the displacement index, we predicted how an SUV curve would have continued without a displacement drug based on a control curve, and compared the prediction to the measured displacement SUV curve. Therefore, the displacement values are susceptible to reproducibility-related errors.

In the control scans, ^{18}F-FP-(+)-DTBZ uptake is pronounced in the pancreas, while the tracer rapidly cleared from the candidate reference regions, spleen and renal cortex, for both ^{18}F-FP-(+)-DTBZ and ^{18}F-FP-(−)-DTBZ. The spleen and renal cortex do not appear to be interchangeable: our PET scans demonstrated higher SUV and V_T in the renal cortex than those in the spleen for both radioligands. The renal pelvis, surrounded by the renal cortex, is a high-activity area in PET imaging for both radiolabeled enantiomers. Given that the size of baboon kidney is small relative to the PET scanner's resolution, the uptake in the renal cortex is likely overestimated by spill-in from the renal pelvis. However, renal cortex SUV was also higher in our *ex vivo* studies where resolution is not an issue. With ^{18}F-FP-(−)-DTBZ, V_T estimates in the renal cortex increased with a longer scan time (Table 3), while V_T estimates in the spleen remained unchanged, suggesting that radiometabolites have a larger effect in the renal cortex than the spleen. Although SUV for the *ex vivo* studies was also higher in the renal cortex than the spleen, as was SUV and V_T from the PET studies, the difference was smaller for parent SUV than for total SUV. This suggests that contribution from radiometabolites partially, but not fully, explains the uptake difference between the spleen and renal cortex.

Experiment results indicated that the SUV of ^{18}F-FP-(+)-DTBZ was higher than that of ^{18}F-FP-(−)-DTBZ (Fig. 3) in the spleen and renal cortex. If no specific binding exists in the renal cortex and spleen, which is a necessary condition for ideal reference regions, the SUV

curves might be expected to show similar kinetics and similar levels for both enantiomers. This difference is not due to a difference in the input functions, though. For example, the uptake in the renal cortex was higher from 60 to 90 min for ^{18}F-FP-(+)-DTBZ with 3.5 ± 0.5 (SUV) than ^{18}F-FP-(−)-DTBZ with 2.6 ± 0.2, while the metabolite-corrected input function from 60 to 90 min was *lower* for ^{18}F-FP-(+)-DTBZ with 0.04 ± 0.01 than ^{18}F-FP-(−)-DTBZ with 0.06 ± 0.01. Also, this difference in the tissue SUV curves cannot be explained solely by the contribution from radiolabeled metabolites. Indeed, in the *ex vivo* radiometabolite study, correcting the SUV to take into account the parent fraction in tissue increased the difference between enantiomers (Table 5).

Another explanation for this difference could be the presence of VMAT2 specific binding in the candidate reference regions, consistent with results from immunohistochemical staining and *in situ* hybridization in humans [19]. Note that there are no available VMAT2 densities reported in the regions. However, when ^{18}F-FP-(+)-DTBZ was displaced by unlabeled FP-(+)-DTBZ (Table 3), no substantial effect was seen in radioactivity uptake in the spleen or renal cortex, indicating that levels of specific binding, if any, are not detectable in either of these putative reference tissues. A remaining possible cause for the different uptake in the spleen and kidney between the enantiomers is the difference in binding to other (non-VMAT2) sites, such as sigma receptors. Since the *in vitro* binding affinity for sigma-1 receptors is similar for both (+)- and (−)- enantiomers of ^{18}F-FP-DTBZ, the sigma binding component is not expected to account for the SUV difference in the renal cortex and spleen between the two enantiomers. Indeed, negligible changes in SUV curves and V_T values (Table 3) were detected from our ^{18}F-FP-(+)-DTBZ fluvoxamine displacement study. Thus, our results suggest the low-affinity sigma-1 receptor binding does not contribute noticeably to the binding in target tissues. In fact, since neither enantiomer of ^{18}F-FP-DTBZ was displaced by either enantiomer of unlabeled FP-DTBZ in spleen or kidney (Table 3), we found no evidence of any specific binding in these potential reference regions. Thus, the difference of the uptake in the spleen and renal cortex between two enantiomers cannot be attributed to the abovementioned causes.

The pancreatic V_T of ^{18}F-FP-(−)-DTBZ might not be a simple indicator of ^{18}F-FP-(+)-DTBZ V_{ND} in the pancreas. Based on our results, we therefore hypothesize that the level of nonspecific binding (V_{ND}) is in fact different between the two enantiomers. If so, it would still be expected that there would be a fixed ratio of the V_{ND} values between enantiomers. This motivated the third method described above using scaled V_T values from the presumed reference regions to estimate V_{ND} and BP_{ND} in the pancreas.

In the above discussion, it should be noted that we had only 1 baboon for PET scans and 1 baboon for radiometabolite measurement with ^{18}F-FP-(−)-DTBZ. Since the number of samples is small, inter-subject variability cannot be excluded, which means that the difference in SUV or parent SUV may just be a result of individual difference among the animals. Note that uptake levels of ^{18}F-FP-(−)-DTBZ in the renal cortex and spleen were not presented in the previous baboon study [9].

In the baboon study of Harris et al. [9], the pancreatic V_T(−) was considered to be similar to V_T(+) in both the spleen and kidney. However in the present study, we found that both V_T(−)

and SUV(−) in the pancreas were lower than V_T(+) and SUV(+) in either the spleen or renal cortex. On the other hand, V_T(−) and SUV(−) in the pancreas were both higher than those in the spleen, and lower than those the renal cortex. Our results indicate the lack of an ideal reference region for quantifying VMAT2 binding in the pancreas, and also reflect the heterogeneity of V_{ND} among regions. In fact, it is not surprising that different organs have different V_T values for a given tracer, even with no specific binding, simply due to differences in tissue characteristics.

We thus compared three methods to estimate V_{ND} values to calculate BP_{ND} of the pancreas. In the first method, the conventional approach, the V_T(+) in the candidate reference region was directly used to estimate V_{ND}. Given the high inter-subject variability (COV) of BP_{ND}, lowest parent fraction in tissue among all regions, and spill-in effect from renal pelvis, the renal cortex is not suitable for a reference region in baboons. Since the uptake in spleen is unaffected by renal damage induced by diabetes, it might be a more suitable region for V_{ND} estimate. In method two, V_T(−) in the pancreas is used directly as a V_{ND} estimate, assuming ideal behavior of the inactive enantiomer. Since this method produced the highest inter-subject variability in BP_{ND} (>30%), it is also not recommended.

The third method accounted for regional and enantiomeric differences. Specifically, it uses a scaled spleen V_T value as V_{ND}; this is similar mathematically to the method previously reported for a brain PET imaging study with ^{11}C-LY2795050 [20], a kappa opioid receptor (KOR) antagonist. Given no suitable reference regions for ^{11}C-LY2795050, the region with the lowest V_T was used to estimate V_{ND}. V_{ND} value from a blocking study with naltrexone was compared to cerebellum V_T to obtain a population-based scale factor between the two values, and V_{ND} values for individual scans were calculated by using that scale factor and individual cerebellum V_T values. In the present study, we assumed that the ratio of pancreas V_{ND} to spleen V_{ND} is a constant between ^{18}F-FP-(+)-DTBZ and ^{18}F-FP-(−)-DTBZ. The inter-scan variability of this scale factor, α_{spleen}, was extremely low (6%), supporting the utility of this approach. Also, the inter-subject variability of BP_{ND} (21%) was lower than or similar to those from the other methods. In order to further evaluate the validity of this method, we are currently conducting studies in T1DM patients and healthy human subjects using PET imaging with both ^{18}F-FP-(+)-DTBZ and ^{18}F-FP-(−)-DTBZ.

5. Conclusion

Differences in distribution volumes among organs between ^{18}F-FP-(+)-DTBZ and ^{18}F-FP-(−)-DTBZ indicated that there are no ideal reference regions for VMAT2 quantification in the pancreas. The PET signal of the renal cortex appeared to be confounded by several factors, including the partial volume effect and radiometabolites. In contrast, spleen radiometabolites make a minor contribution relative to that of the parent ^{18}F-FP-(+)-DTBZ, and the dimensions of the spleen minimize quantification errors due to partial volume effects. Thus, the spleen is deemed a more practical candidate for use as a pseudo-reference region. Here, we propose to use a scaled spleen V_T value as V_{ND} to compute pancreatic BP_{ND} using ^{18}F-FP-(+)-DTBZ.

Supplementary Material

Refer to Web version on PubMed Central for supplementary material.

Acknowledgments

The authors appreciate the excellent technical assistance of the staff at the Yale University PET Center. The authors appreciate many fruitful discussions with Dr. Jean-Dominique Gallezot. This study was supported by JDRF 37-2011-633.

References

[1]. Butler AE, Janson J, Bonner-Weir S, Ritzel R, Rizza RA, Butler PC. Beta-cell deficit and increased beta-cell apoptosis in humans with type 2 diabetes. Diabetes. 2003; 52:102–10. [PubMed: 12502499]

[2]. Wang X, Misawa R, Zielinski MC, Cowen P, Jo J, Periwal V, et al. Regional differences in islet distribution in the human pancreas—preferential beta-cell loss in the head region in patients with type 2 diabetes. PLoS One. 2013; 8:e67454. [PubMed: 23826303]

[3]. Souza F, Simpson N, Raffo A, Saxena C, Maffei A, Hardy M, et al. Longitudinal noninvasive PET-based beta cell mass estimates in a spontaneous diabetes rat model. J Clin Invest. 2006; 116:1506–13. [PubMed: 16710474]

[4]. Anlauf M, Eissele R, Schafer MK, Eiden LE, Arnold R, Pauser U, et al. Expression of the two isoforms of the vesicular monoamine transporter (VMAT1 and VMAT2) in the endocrine pancreas and pancreatic endocrine tumors. J Histochem Cytochem. 2003; 51:1027–40. [PubMed: 12871984]

[5]. Harris PE, Ferrara C, Barba P, Polito T, Freeby M, Maffei A. VMAT2 gene expression and function as it applies to imaging beta-cell mass. J Mol Med (Berl). 2008; 86:5–16. [PubMed: 17665159]

[6]. Maffei A, Liu Z, Witkowski P, Moschella F, Del Pozzo G, Liu E, et al. Identification of tissue-restricted transcripts in human islets. Endocrinology. 2004; 145:4513–21. [PubMed: 15231694]

[7]. Saisho Y, Harris PE, Butler AE, Galasso R, Gurlo T, Rizza RA, et al. Relationship between pancreatic vesicular monoamine transporter 2 (VMAT2) and insulin expression in human pancreas. J Mol Histol. 2008; 39:543–51. [PubMed: 18791800]

[8]. Normandin MD, Petersen KF, Ding YS, Lin SF, Naik S, Fowles K, et al. In Vivo imaging of endogenous pancreatic beta-cell mass in healthy and type 1 diabetic subjects using F-18-fluoropropyl-dihydrotetrabenazine and PET. J Nucl Med. 2012; 53:908–16. [PubMed: 22573821]

[9]. Harris PE, Farwell MD, Ichise MPET. Quantification of pancreatic VMAT 2 binding using (+) and (−) enantiomers of [^{18}F]FP-DTBZ in baboons. Nucl Med Biol. 2013; 40:60–4. [PubMed: 23102539]

[10]. Kung MP, Hou C, Lieberman BP, Oya S, Ponde DE, Blankemeyer E, et al. In Vivo imaging of beta-cell mass in rats using ^{18}F-FP-(+)-DTBZ: a potential PET ligand for studying diabetes mellitus. J Nucl Med. 2008; 49:1171–6. [PubMed: 18552132]

[11]. Singhal T, Ding YS, Weinzimmer D, Normandin MD, Labaree D, Ropchan J, et al. Pancreatic beta cell mass PET imaging and quantification with [^{11}C]DTBZ and [^{18}F]FP-(+)-DTBZ in rodent models of diabetes. Mol Imaging Biol. 2011; 13:973–84. [PubMed: 20824509]

[12]. Kung MP, Hou C, Goswami R, Ponde DE, Kilbourn MR, Kung HF. Characterization of optically resolved 9-fluoropropyl-dihydrotetrabenazine as a potential PET imaging agent targeting vesicular monoamine transporters. Nucl Med Biol. 2007; 34:239–46. [PubMed: 17383573]

[13]. Tsao HH, Skovronsky DM, Lin KJ, Yen TC, Wey SP, Kung MP. Sigma receptor binding of tetrabenazine series tracers targeting VMAT2 in rat pancreas. Nucl Med Biol. 2011; 38:1029–34. [PubMed: 21982574]

[14]. Viola P, Wells WM III. Alignment by maximization of mutual information. Int J Comput Vision. 1997; 24:137–54.

[15]. Ichise M, Toyama H, Innis RB, Carson RE. Strategies to improve neuroreceptor parameter estimation by linear regression analysis. J Cereb Blood Flow Metab. 2002; 22:1271–81. [PubMed: 12368666]

[16]. Innis RB, Cunningham VJ, Delforge J, Fujita M, Gjedde A, Gunn RN, et al. Consensus nomenclature for in vivo imaging of reversibly binding radioligands. J Cereb Blood Flow Metab. 2007; 27:1533–9. [PubMed: 17519979]

[17]. Rahier J, Goebbels RM, Henquin JC. Cellular composition of the human diabetic pancreas. Diabetologia. 1983; 24:366–71. [PubMed: 6347784]

[18]. Wang X, Zielinski MC, Misawa R, Wen P, Wang TY, Wang CZ, et al. Quantitative analysis of pancreatic polypeptide cell distribution in the human pancreas. PLoS One. 2013; 8:e55501. [PubMed: 23383206]

[19]. Anlauf M, Schafer MK, Schwark T, von Wurmb-Schwark N, Brand V, Sipos B, et al. Vesicular monoamine transporter 2 (VMAT2) expression in hematopoietic cells and in patients with systemic mastocytosis. J Histochem Cytochem. 2006; 54:201–13. [PubMed: 16116033]

[20]. Naganawa M, Zheng MQ, Nabulsi N, Tomasi G, Henry S, Lin SF, et al. Kinetic modeling of ^{11}C-LY2795050, a novel antagonist radiotracer for PET imaging of the kappa opioid receptor in humans. J Cereb Blood Flow Metab. 2014; 34:1818–25. [PubMed: 25182664]

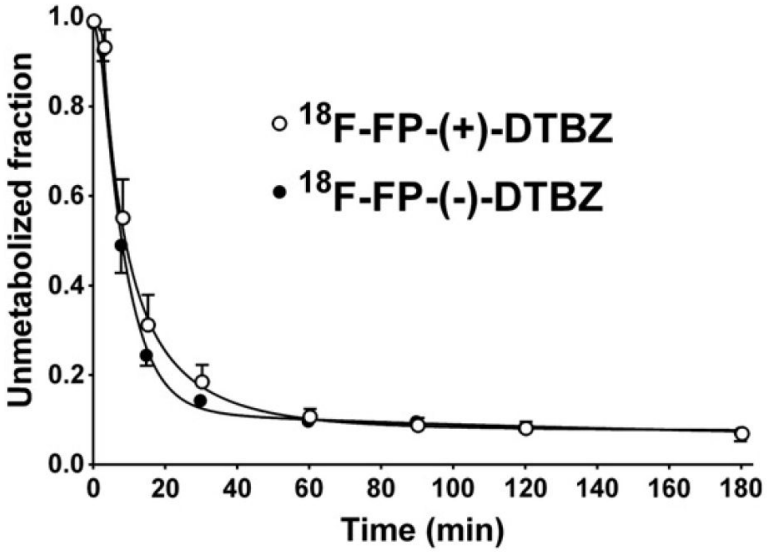

Fig. 1.

Mean ± SD of unmetabolized fraction in the plasma over time after injection of ^{18}F-FP-(+)-DTBZ (open circles, $n = 8$) and ^{18}F-FP-(−)-DTBZ (closed circles, $n = 3$).

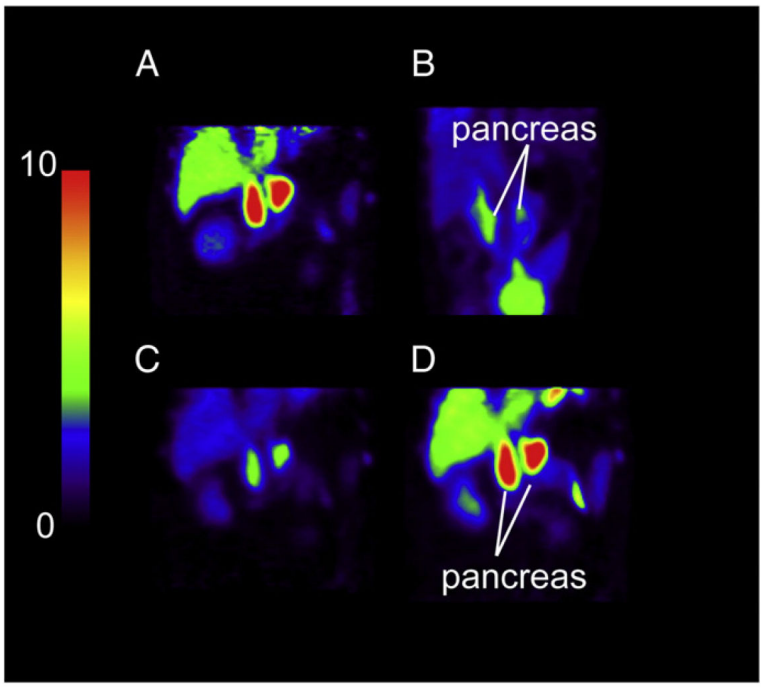

Fig. 2.

PET SUV images after injection of ^{18}F-FP-(+)-DTBZ (A, C, and D) and ^{18}F-FP-(−)-DTBZ (B). All images are displayed on the same SUV scale. A, C, D: PET images, summed from 120 to 150 min, from the same baboon (Baboon B) scanned with ^{18}F-FP-(+)-DTBZ under control condition (A) and following displacement by unlabeled FP-(+)-DTBZ (C) and fluvoxamine (D). B: PET images of ^{18}F-FP-(−)-DTBZ summed from 0 to 90 min (Baboon D).

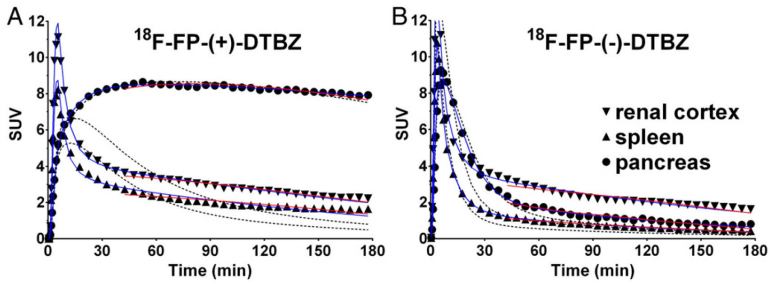

Fig. 3.

Examples of regional time–activity curves in the baboon abdomen for control scans with ^{18}F-FP-(+)-DTBZ (A) and ^{18}F-FP-(−)-DTBZ (B). Curve fittings shown are with one-tissue (black dotted curve) and two-tissue (blue curve) compartment models, as well as the multilinear analysis 1 method (red curve). Radioactivity concentrations are expressed in SUV units (concentration/ (injected dose/body weight)).

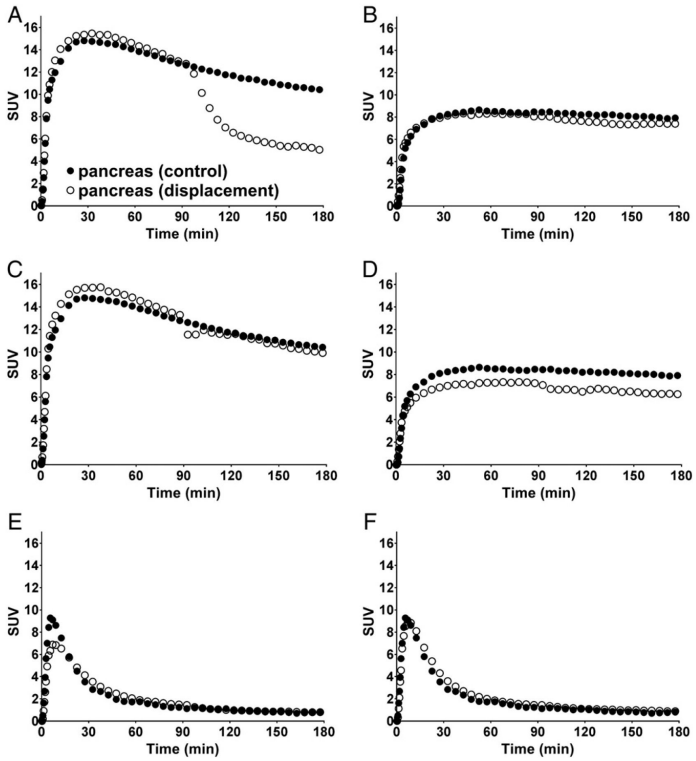

Fig. 4.

Time–activity curves (TACs) in the pancreas from a control scan (closed circles) and a displacement scan (open circles) of ^{18}F-FP-(+)-DTBZ (A–D) and ^{18}F-FP-(−)-DTBZ (E and F). Displacing agents are unlabeled FP-(+)-DTBZ (0.5 mg/kg) (A and E), unlabeled FP-(−)-DTBZ (0.5 mg/kg) (B and F), and fluvoxamine (3 mg/kg) (C and D), administered as an i.v. bolus at 90 min after radioligand injection. For the fluvoxamine displacement study, TACs from the displacement portions of the scan were corrected for body motion. Radioactivity concentrations are expressed in SUV units (concentration/ (injected dose/body weight)).

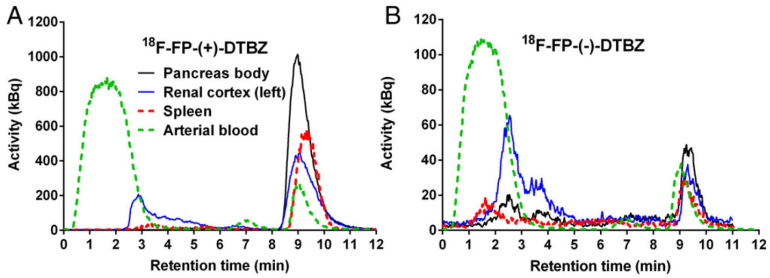

Fig. 5.

Representative HPLC chromatograms of plasma and tissue extracts at 90 min post-injection of (A) ^{18}F-FP-(+)-DTBZ and (B) ^{18}F-FP-(−)-DTBZ. The parent tracer has a retention time of ~9 min. Earlier eluting peaks are radiometabolites.

Table 1

Study summary.

	Displacing agents	Radioligands	
		^{18}F-FP-(+)-DTBZ	^{18}F-FP-(−)-DTBZ
Displacement study	saline (control)	Baboons A, B, and C	Baboon D
	FP-(+)-DTBZ	Baboons A (0.25 mg/kg) and B (0.5 mg/kg)	Baboon D (0.5 mg/kg)
	FP-(−)-DTBZ	Baboon C (0.5 mg/kg)	Baboon D (0.5 mg/kg)
	fluvoxamine	Baboons B and C (3 mg/kg)	
Tissue radiometabolite measurement		Baboons C and E	Baboon F

Table 2

Distribution volume (V_T) values.

Regions	V_T (mL/cm^3)							
	^{18}F-FP-(+)-DTBZ (n = 3)				^{18}F-FP-(−)-DTBZ (n = 1)			
	90 min[a]	120 min	180 min	240 min	90 min[a]	120 min	180 min	240 min
Pancreas	158 ± 48	170 ± 22	190 ± 29	205 ± 44	19 ± 2	19	20	20
Renal cortex	43 ± 12	43 ± 7	46 ± 7	48 ± 7	28 ± 1	29	32	33
Spleen	25 ± 7	25 ± 5	29 ± 6	31 ± 8	12 ± 1	12	12	12

Data are derived from MA1 model and expressed as mean ± SD.

[a]For 90 min data, n = 8(^{18}F-FP-(+)-DTBZ) and n = 3(^{18}F-FP-(−)-DTBZ).

Table 3

Reduction in the SUV by displacing agents.

Tracers	Displacing agents								
	FP-(+)-DTBZ			FP-(−)-DTBZ			fluvoxamine		
	Pancreas	Renal cortex	Spleen	Pancreas	Renal cortex	Spleen	Pancreas	Renal cortex	Spleen
^{18}F-FP-(+)-DTBZ	36 ± 17%[a]	−9 ± 21%[a]	9 ± 3%[a]	7%[b]	1%[b]	3%[b]	6 ± 1%[c]	−11 ± 13%[c]	9 ± 4%[c]
^{18}F-FP-(−)-DTBZ	14%[b]	0%[b]	−11%[b]	−1%[b]	12%[b]	0%[b]			

[a] 0.5 mg/kg (n = 1) and 0.25 mg/kg (n = 1).

[b] 0.5 mg/kg (n = 1).

[c] 3 mg/kg (n = 2).

Table 4

Non-displaceable distribution volume (V_{ND}) and pancreatic BP_{ND} estimated from 90 min of scan data.

Method	V_{ND}	α	Pancreatic BP_{ND}(+) (n = 8)
1. V_{ND} = V_T(+, spleen)	25 (29%)		5.3 (19%)
1. V_{ND} = V_T(+, renal cortex)	43 (27%)		2.7 (30%)
2. V_{ND} = V_T(−, pancreas)	19 (9%)		7.1 (34%)
3. V_{ND} = V_T(+, spleen)/α_{spleen}	39 (29%)	0.64 (6%)	3.0 (21%)
3. V_{ND} = V_T(+, renal cortex)/α_{renal}	29 (27%)	1.48 (10%)	4.5 (27%)

Data are derived from MA1 model and expressed as mean (COV%).

Table 5

SUV and unmetabolized parent fractions.

		^{18}F-FP-(+)-DTBZ (n = 2)[a]			^{18}F-FP-(−)-DTBZ (n = 1)		
Region	**Subregion**	**SUV**	**Parent fraction (%)**	**Parent SUV**	**SUV**	**Parent fraction (%)**	**Parent SUV**
Arterial Plasma		0.5 ± 0.1	10 ± 2	0.05 ± 0.00	0.8	5	0.04
Pancreas	Head	12.1 ± 5.4	99 ± 2	12.0 ± 5.5	1.0	59	0.6
	Uncinate	12.8 ± 4.5	98 ± 1	12.6 ± 4.6	1.0	63	0.6
	Neck	12.9 ± 4.6	99 ± 1	12.8 ± 4.7	1.0	49	0.5
	Body	16.1 ± 9.2	99 ± 2	16.0 ± 9.3	1.1	63	0.7
	Tail	13.1 ± 4.8	98 ± 1	12.9 ± 4.9	1.1	47	0.5
Renal Cortex	Left	5.4 ± 1.9	70 ± 8	3.7 ± 0.9	3.0	25	0.8
	Right	6.3[b]	71 ± 9	4.1[b]	3.1	32	1.0
Spleen		3.2 ± 0.3	94 ± 2	3.0 ± 0.2	1.0	53	0.5
Liver		3.3 ± 0.6	59 ± 5	2.0 ± 0.2	1.2	36	0.4
Brain	Cerebellum	1.3 ± 0.1	93 ± 1	1.2 ± 0.1			
	Frontal cortex	1.6 ± 0.01	94 ± 5	1.5 ± 0.1			
	Putamen	11.8[b]	100[b]	11.8[b]			
	Caudate	13.5[b]	99[b]	13.4[b]			

[a] Data are mean ± SD.

[b] n = 1.